The effect of high-pressure plastic forming on the structure and strength of AA5083 and AA5754 alloys intended for fasteners

M. KULCZYK*, J. SKIBA, W. PACHLA, J. SMALC-KOZIOROWSKA,
S. PRZYBYSZ, and M. PRZYBYSZ

Institute of High Pressure Physics of the Polish Academy of Sciences UNIPRESS, Sokolowskis 29/37, 01-142 Warsaw, Poland

Abstract. The presented results describe the effect of severe plastic deformation on the structure and mechanical properties of AA5083 and AA5754 alloys. Both materials were subjected to single hydrostatic extrusion (HE) and cumulative hydrostatic extrusion in the case of AA5083 and a combination of plastic deformation by equal-channel angular pressing (ECAP) with the next HE for AA5754. After the deformation, both alloys featured a homogeneous and finely divided microstructure with average grain size deq = 140 nm and 125 nm for AA5083 and AA5754, respectively. The selection of plastic forming parameters enabled a significant increase in the UTS tensile strength and YS yield stress in both alloys – UTS = 510 MPa and YS = 500 MPa for alloy AA5083 after cumulative HE, and 450 MPa and 440 MPa for alloy AA5754 after the combination of ECAP and HE, respectively. It has been shown on the example of AA5083 alloy that after the deformation the threads of the fasteners made of this material are more accurate and workable at lower cutting speeds, which saves the cutting tools. The resultant properties of AA5083 and AA5754 alloys match the minimum requirements for the strongest Al-Zn alloys of the 7xxx series, which, however, due to the considerably lower corrosion resistance, can be replaced in many responsible structures by the AA5xxx series Al-Mg alloys presented in this paper.

Key words: AA5xxx series, ultra high mechanical properties, hydrostatic extrusion, grain refinement, workability tests.

1. Introduction

The 5xxx series aluminium and magnesium alloys are characterized by very good corrosion resistance, good weldability, and machinability, as well as impact strength in cryogenic conditions [1–4]. They are commonly used in the maritime industry for structural elements and fittings, for fuel tanks, and in the automotive industry [2–3]. Their main applicability limitation is not very high strength of this group of alloys. The 5xxx alloys cannot be strengthened by heat treatment, hence the only way to improve their mechanical properties is plastic forming, such as rolling [3]. These alloys are also used for fasteners in less critical structures carrying lower loads at the UTS strength level of ∼200 MPa, i.e. nearly three times lower than the strongest 7xxx series aluminium alloys with zinc [5]. However, the 5xxx alloys are in several ways better than the 7xxx series, as they have low density, good plasticity, low alloying content, and single-phase structure free of particles [6]. This work concerns the elimination of the Al-Mg alloys' disadvantage of relatively low strength. To do this, it is planned to use the severe plastic deformation SPD method, i.e. the hydrostatic extrusion HE method and its combination with the equal-channel angular pressing ECAP. The effectiveness of HE as a process leading to a strong refinement of the microstructure was widely presented for such materials

as copper, aluminium, magnesium, as well as nickel and titanium alloys, and acid-resistant steel [7–14]. For AA5483 alloy in small products in the form of rods with a less than 5 mm diameter, the combination of ECAP and HE processes resulted in a finely grained nanostructure with grains below 100 nm [4]. In this study two Al-Mg AA5083 and AA5754 alloys will be tested. Until now, according to the relevant literature, mainly ECAP or high pressure torsion HPT have been used as SPD deformation for these alloys [6, 15–17]. AA5083 alloy was ECAP deformed in C route at 100°C, which after 8 passes produced the microstructure refinement to ∼300 nm with tensile strength UTS ∼450 MPa [17]. Cold ECAP of AA5754 alloy in Bc route resulted after 5 passes in the UTS ∼390 MPa and the grain size ∼300–400 nm [16]. Because of the small size of its products, the HPT method is not suitable for the production of prefabricated elements for fasteners. On the other hand, as demonstrated by previous attempts to manufacture structural elements, the HE hydrostatic extrusion process gives hope for its effective commercial application [11, 13]. From the point of view of application of aluminium alloys after SPD processes in fasteners, the literature data mainly indicate the use of the ECAP and the continuous ECAP processes [18–20]. The presented tests concern the AA1050 alloy and the AA6061 alloys. Apart from a comprehensive analysis of mechanical properties, they do not describe issues related to the formability of finely divided materials. This study analyses the effect of high-pressure plastic processing on the mechanical properties and microstructure of AA5083 and AA5754 alloys and describes the impact of these properties on the finished product manufacturing process.

M. Kulczyk, J. Skiba, W. Pachla, J. Smalc-Koziorowska, S. Przybysz, and M. Przybysz

2. Material and experimental

Two alloys of aluminium with magnesium AA5083 and AA5754 were tested. The chemical composition of the tested aluminium alloys is shown in Table 1.

Table 1
Chemical composition (wt%) of the tested aluminium alloys

Content of elements, %wt.									
	Si	Fe	Cu	Mn	Mg	Cr	Zn	Ti	Al
AA 5083	0.15	0.25	0.01	0.7	4.4	0.1	0.03	0.06	balance
AA 5754	0.22	0.39	0.04	0.29	2.84	0.03	0.05	0.01	balance

The alloys were formed according to the following procedures:

a) Both alloys in the form of rods with 70 mm diameter were subjected to a one-step hydrostatic extrusion process with a degree of reduction R, where R is the ratio of the material cross-sections before and after the extrusion process, in the range of $R = 3, 4, 5.2, 6.1$ and 7.4, on end diameters, 40 mm, 35 mm, 30 mm, 28 mm and 26 mm, respectively.

b) AA5083 alloy rods with 70 mm initial diameter were subjected to a four-step cumulative hydrostatic extrusion to 10 mm final diameter (70 mm > 26 mm > 16 mm > 10 mm) with cumulative reduction $R_{cum} \sim 19$, i.e. cumulative true strain $\varepsilon_{cum} = 3.9$.

c) AA5754 alloy rods with 30 mm initial diameter (after machining 70 mm diameter rods) were subjected to a two-step ECAP with 180° rotation between successive passes (route C) and cumulative true strain $\varepsilon = 2.1$, and after the ECAP process the material was subjected to a one-step HE to 16 mm diameter and to a two-step HE to 10 mm diameter with cumulative strain $\varepsilon_{cum} = 2.2$. The total cumulative true strain after ECAP + HE processes was $\varepsilon_{cum} = 4.3$.

Both processes, HE and ECAP, were conducted at room temperature, with $2\alpha = 45°$ HE matrix angle, and $\psi = 90°$ ECAP channel angle. After the HE process and leaving the deformation zone, the material was intensively cooled with water at the exit from the matrix.

The microstructure of the material in the initial state was analysed with a LM Nikon Eclipse LV150 light microscope, and after plastic deformation processes - with a TEM Tecnai TF20 transmission electron microscopy. The extruded bars' cross-sections were subject to the TEM examination. Samples were polished and etched and thin foils intended for TEM observation were prepared. The grain size was quantitatively evaluated using the 'Micrometer' software [21]. Based on TEM images, after at least 200 randomly selected grains from the population, the grains were outlined and software calculation of the equivalent grain diameter d_{eq} was made, where d_{eq} is defined as a diameter of a circle with the surface area equal to a given grain. Mechanical properties were determined with a Zwick/Roell Z250 kN universal tensile unit in a static tensile test at the room temperature, with 0.008 s^{-1} strain rate, and length to diameter ratio equal 5. The material hardness was measured by Vickers HV10 method on an automated KB 250 BVRZ hardness tester with 10 kG load and 15 s test period.

The AA5083 alloy threadability was analysed by plastic forming and machining methods with a HAAS ST30Y 3-axis machine tool. The test involved AA5083 alloy in the initial state and after the HE process, of which M30 metric threads were made in accordance with PN-ISO 965–2: 2001 standard for ordinary external threads, which corresponds to the medium-exact thread class.

Thread burnishing was tested with an LMT FETTE FU 4–1 head in the range of thread profiles from M14 to M30 at $n = 80$ rev/min speed. Thread cutting was tested with a tool consisting of a STGCR 1616H11-B1 holder on which a TCGX 110302-AL H10 insert was mounted. The threads were cut at three different speeds $n = 500, 1000$ and 1500 rev/min, which correspond to cutting speeds Vc 47, 94 and 142 m/min, respectively. The threaded bolts were subjected to geometric analysis using a Sinpo-Profile Projector JT12A-B measuring microscope. The following thread dimensions: outer diameter d, pitch diameter $d2$, and inner diameter $d3$ were determined according to PN-ISO 965–2: 2001 standard for general purpose metric threads.

3. Results and discussion

3.1. Hydrostatic extrusion process. Figure 1 shows sample characteristics of the one-step process of HE extrusion of AA5083 and AA5754 alloys with $\varepsilon = 2$ maximum unit true strain. In the initial phase of the HE process, an increase in pressure is observed, associated with compressing the pressure medium in the working chamber to a value that allows the process of the material's plastic flow to start. The pressure peak is associated with the commencement of the material flow and the change of static to kinetic friction followed by the stabilization of the extrusion pressure and material outflow at a constant
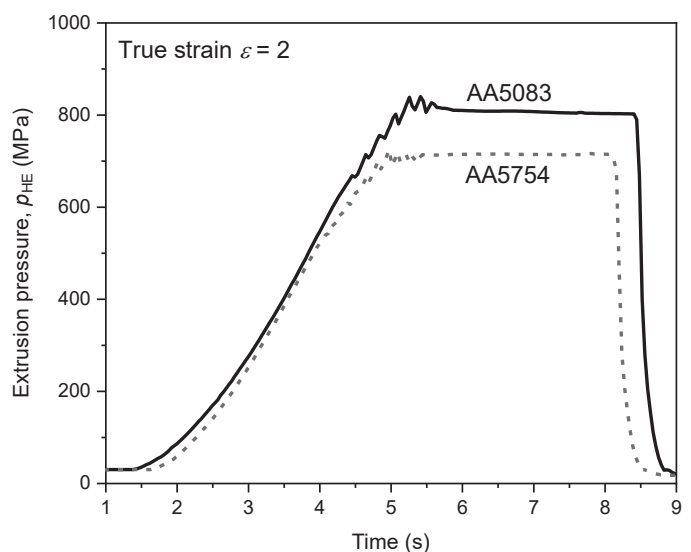

Fig. 1. Characteristics of the one-step hydrostatic extrusion HE of AA5083 and AA5754 alloys with true strain $\varepsilon = 2$
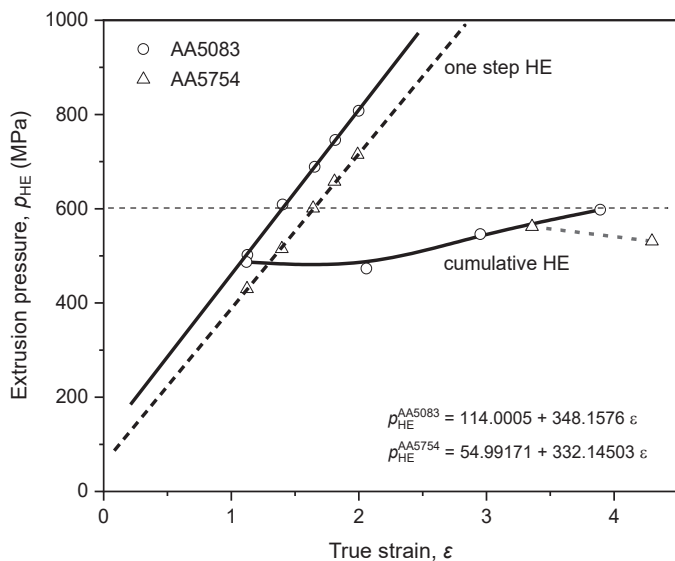
www.czasopisma.pan.pl   www.journals.pan.pl

The effect of high-pressure plastic forming on the structure and strength of AA5083 and AA5754 alloys intended for fasteners

Fig. 2. Dependence of extrusion pressure on true strain for the one-step and cumulative cold hydrostatic extrusion of AA5083 and AA5754 alloys

Fig. 3. Dependence of UTS tensile strength and YS yield stress on true strain ε for AA5083 alloy after the one-step cold hydrostatical extrusion HE and after the cumulative extrusion

extrusion rate. Obtaining a constant extrusion speed is important for the homogeneity of physical and mechanical properties over the length of the extruded product.

Figure 2 shows the dependence of extrusion pressure as a function of true strain $\varepsilon = \ln R$, where R is the reduction degree, for both alloys at one-step and cumulative extrusion (in several subsequent passes). The best from the economic point of view would be a one-step HE, but it significantly limits the deformation applicable due to the significant increase in extrusion pressures, even at true strain $\varepsilon \sim 2$ to $p_{HE} \sim 800$ MPa and 700 MPa, for AA5083 and AA5754, respectively. The high pressures generate strong adiabatic heating effects that activate the healing and recrystallization processes limiting the deformation strengthening of materials, in particular the materials with low melting point and temperature sensitivity, such as aluminium alloys. With the cumulative HE, i.e. several sequential steps of extrusions of the same material, the unit extrusion pressures can be significantly reduced, and thus also the adiabatic heating effect, with a higher cumulative true strain. The maximum extrusion pressure for both cumulatively extruded alloys do not exceed $p_{HE} = 600$ MPa with cumulative deformation nearly twice as high, i.e. $\varepsilon_{cum} = 3.9$ for AA5083 alloy, and more than twice as high, i.e. $\varepsilon_{cum} = 4.3$ for AA5754 alloy previously subjected to ECAP by route C.

3.2. Mechanical properties. Figure 3 shows the effect of deformation on UTS tensile strength and YS yield strength of AA5083 alloy. The $\varepsilon > 1.3$ strain in a single HE step leads to a continuous decrease in both mechanical properties to strain $\varepsilon \sim 2$, which proves permanent leveling of the deformation strengthening due to the increasing adiabatic heating effects and the thereby caused healing and recrystallization processes. The yield strength from the maximum YS = 370 MPa decreased by over 15% to YS = 310 MPa with $\varepsilon \sim 2$ strain. The UTS
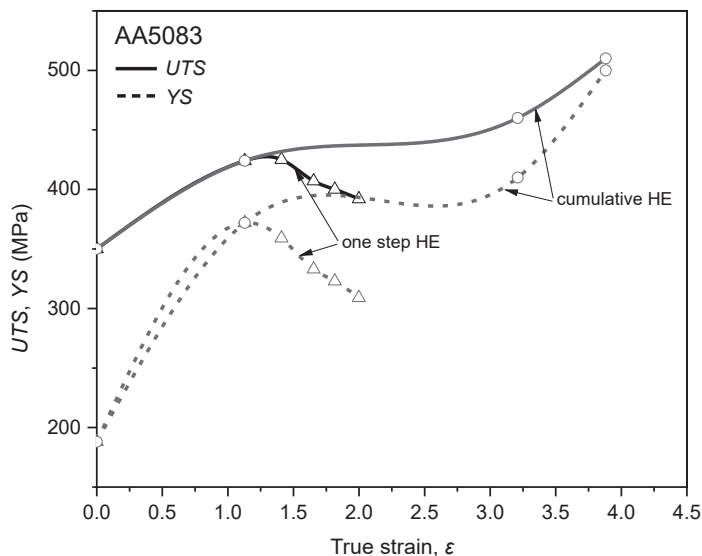
decreased similarly, but the percentage was half as low, from the maximum UTS = 425 MPa to UTS = 392 MPa. In contrast to the one-step HE, the cumulative HE causes the UTS and YS to increase to the maximum cumulative strain $\varepsilon_{cum} \sim 4$, at which they reach the highest values: UTS = 510 MPa and YS = 500 MPa at elongation to break $\varepsilon_f = 6\%$.

Figure 4 shows a comparison of the mechanical properties of AA5083 alloy with the initial material before plastic working and with the mechanical parameters required for fasteners from the strongest group of AA7075 aluminium alloys with zinc [5]. The cumulative hydrostatic extrusion HE of AA5083 alloy produced mechanical properties similar to or even higher
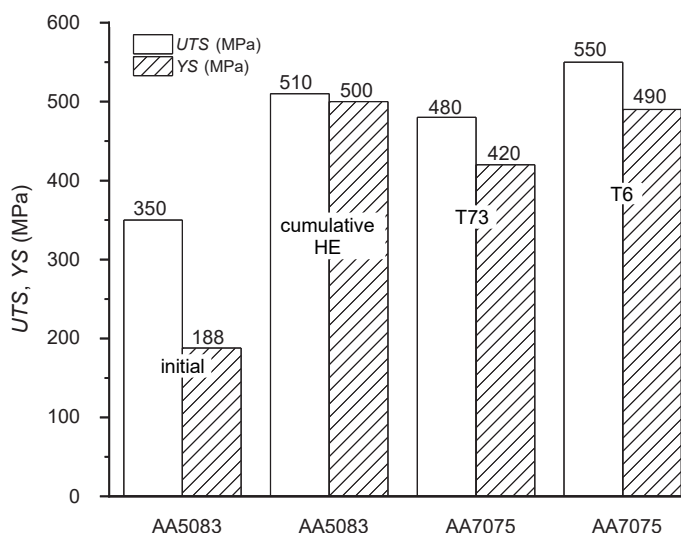

Fig. 4. Comparison of UTS tensile strength and YS yield stress of the AA5083 alloy after the cumulative HE hydrostatic extrusion process with the initial material and minimum commercial alloy requirements for fasteners AA7075 in the T73 and T6 state [5]

than those of AA7075 alloy, characterized by significantly lower corrosion resistance and, for the purpose of strengthening, the need for precipitation hardening in supersaturation and ageing processes. Compared to the initial material, the cold cumulative HE increased YS by ca. 175% and UTS by 45%, i.e. in excess of 500 MPa (Fig. 4), whereas engineering requirements for fasteners made of 5xxx aluminium alloys indicate the minimum strength of UTS = 200 MPa [5]. A similar nature of changes in mechanical properties as a function of the deformation degree was observed for AA5754 alloy (Fig. 5). At the one-step HE process with a strain increase after exceeding $\varepsilon \sim 1.3$, practically no changes are observed in UTS tensile strength, which oscillates around UTS ~ 370 MPa, and YS yield strength drops by $\sim 10\%$ reaching YS = 310 MPa at strain $\varepsilon \sim 2$. On the other hand, when the process of one-step HE with true strain $\varepsilon \sim 1.2$ was preceded with two-step ECAP by C route, the mechanical properties improved dramatically to UTS = 430 MPa and YS = 410 MPa. With the repeated HE extrusion with $\varepsilon \sim 1$ accumulating the true strain cumulative $\varepsilon_{cum} = 4.3$, the maximum mechanical parameters were achieved, i.e. UTS = 450 MPa and YS = to 440 MPa, i.e. higher by $\sim 20\%$ and $\sim 30\%$, respectively, compared to the values for the HE process with strain $\varepsilon = 1.2$ alone (Fig. 5). At this strength, the elongation to break of the final product was $\varepsilon_f = 5\%$. For AA5754 alloy, as for AA5083 alloy, a very large increase is observed in the mechanical properties compared to the initial material not subjected to plastic working by ECAP and HE methods, for which YS increases by nearly 170% and UTS by about 60% (Fig. 6). It is worth noting that after adding the ECAP process to HE, the difference between UTS and YS decreases to ~ 10 MPa, which means that a fastener made of such a material can be safely loaded as much as its strength allows. Figure 6 also shows literature data for AA5754 alloy

Fig. 6. Comparison of UTS tensile strength and YS yield stress of AA5754 alloy after the cold cumulative HE hydrostatic extrusion and the combination of ECAP and HE processes, with the initial material and literature data for multi-step ECAPx6 and ECAPx5 processes [15, 16]

after five- and six-step ECAP processes by Bc route, for which the strength increased by $\sim 20\%$ only compared to the initial material [15, 16].

3.3. Hardness. Figure 7 shows the changes in the average HV10 hardness of AA5083 and AA5754 alloys as a function of true strain ε after the cold cumulative HE and its combination with the ECAP process. In the AA5083 alloy, the highest HV surge of over 50% is observed after the first extrusion step,
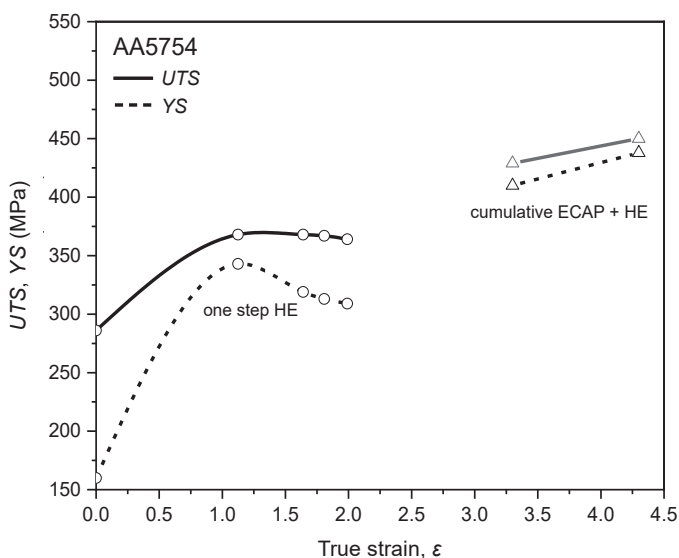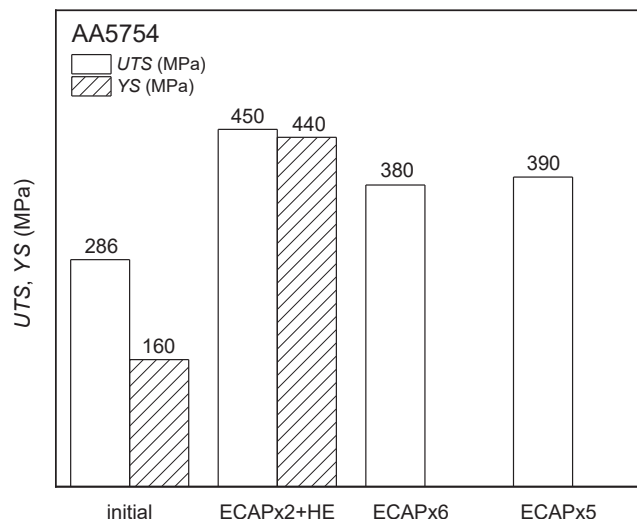

Fig. 5. Dependence of UTS tensile strength and YS yield stress on true strain ε for AA5754 alloy after the one-step cold hydrostatic extrusions, and after the cumulative HE followed by the two-step ECAP by route C and the subsequent one- and two-step HE processes
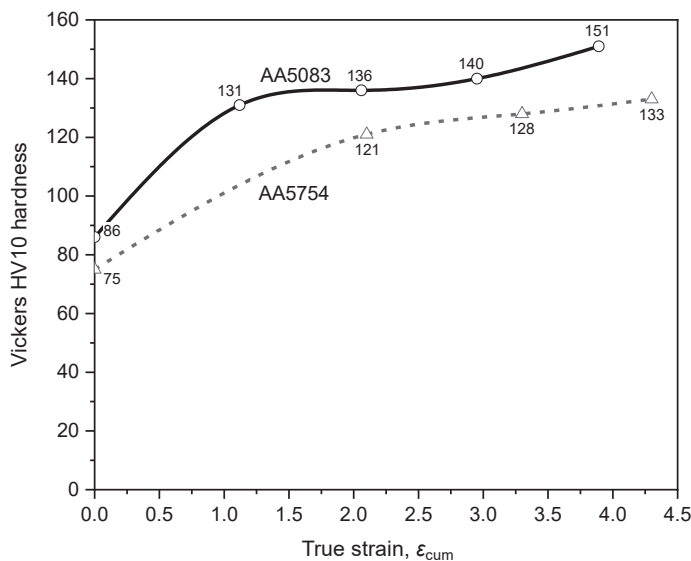

Fig. 7. Change in Vickers HV10 hardness as a function of cumulative true strain ε_{cum} for AA5083 alloy after the cold cumulative HE, and for AA5754 alloy after the process of subsequent cumulative two-step ECAP, two-step ECAP and one-step HE, and two-step ECAP and two-step HE

www.czasopisma.pan.pl   PAN   www.journals.pan.pl
POLSKA AKADEMIA NAUK

The effect of high-pressure plastic forming on the structure and strength of AA5083 and AA5754 alloys intended for fasteners
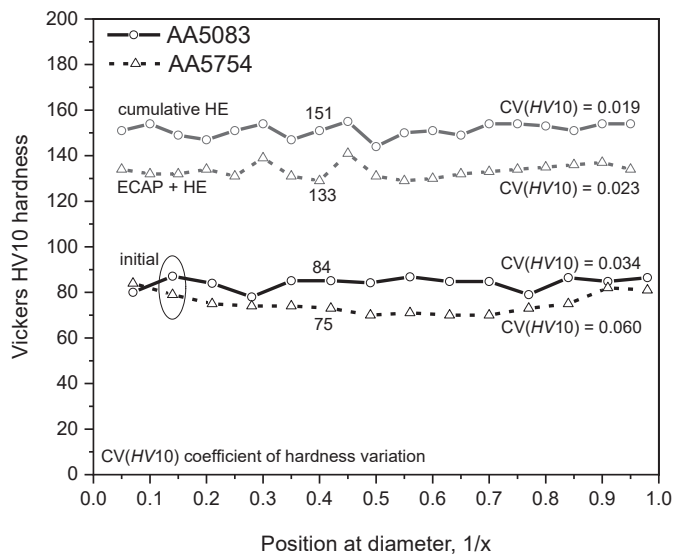
Fig. 8. Comparison of the HV10 microhardness distribution over the cross section for AA5083 alloy after the cold cumulative HE extrusion process with cumulative true strain $\varepsilon_{cum} = 3.9$ and for AA5754 alloy after the ECAP + HE process with cumulative strain $\varepsilon_{cum} = 4.3$ with the initial materials

followed by a further steady increase to the maximum value of 151HV10, i.e. an increase by over 75%, with cumulative true strain $\varepsilon = 3.9$. This is typical of the HE process, in which after the first step of extrusion, the material gets saturated with defects resulting from high plastic deformation, but in subsequent deformation steps the generation of structural defects and their annihilation as a result of adiabatic heating become more balanced. This phenomenon is particularly evident in materials susceptible to thermal effects, such as aluminium alloys, in which, despite intensive cooling, along with its deformation strengthening the material is subjected to processes that weaken the strengthening effects, such as dynamic recovery. The AA 5754 alloy shows an increase in hardness after the two-step ECAP process to 121HV10, and further on, following the two-step HE process, the maximum of 133HV10 is reached, representing an increase by nearly 80% compared to the initial material. Figure 8 shows the hardness distribution over the cross-section of AA5083 alloy bars, in their initial state and after the cold HE process with $\varepsilon_{cum} = 3.9$, illustrating the improvement in the homogeneity of the bar microstructure after HE as evidenced by the lower values of the coefficient of microhardness variation CV (HV10) compared to the initial material. A similar nature of hardness changes was observed for AA5754 alloy after the combination of ECAP and HE processes with cumulative true strain $\varepsilon_{cum} = 4.3$ (Fig. 8). After the plastic deformation process, a clearly more homogeneous distribution of hardness is observed, as evidenced by almost twice lower CV (HV10), and the average hardness value increases by almost 80% compared to the initial material.

3.4 Microstructure. The initial AA5083 alloy was characterized by a coarse grained structure with an average grain size $d_{eq} \sim 50$ μm (Fig. 9a). After the three-step cumulative cold
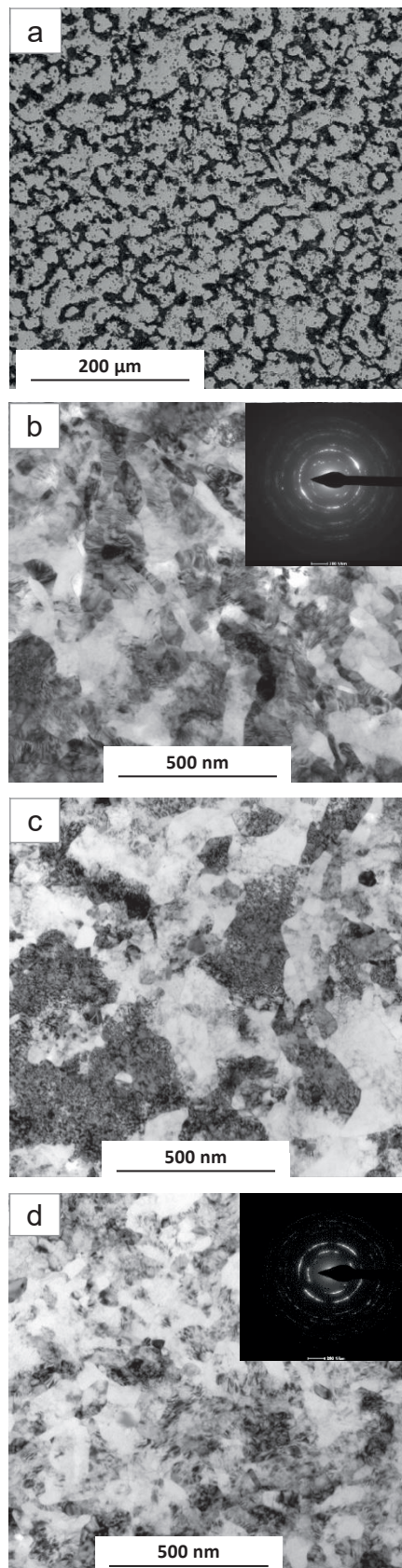

Fig. 9. AA5083 alloy microstructure on the cross-section of the rod (a) in the initial state, (b) and (c) after the cold cumulative HE extrusion with cumulative strain $\varepsilon_{cum} \sim 2.95$, and (d) after the cumulative HE process with $\varepsilon_{cum} \sim 3.9$
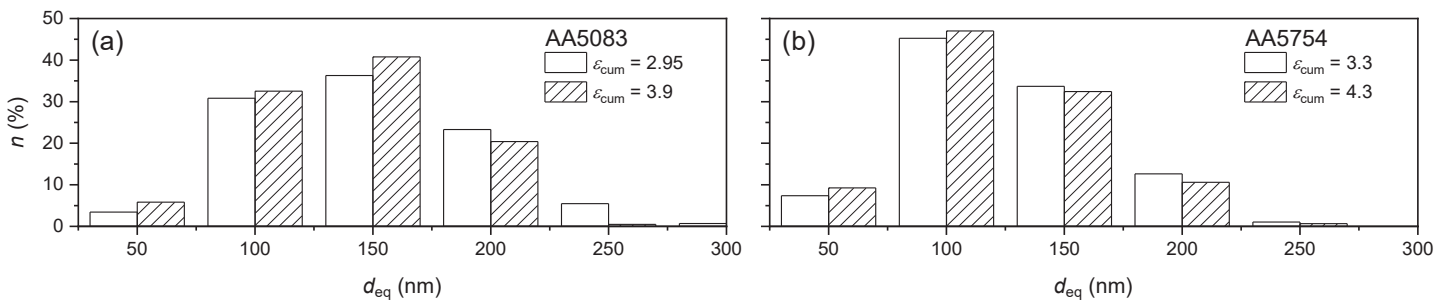
M. Kulczyk, J. Skiba, W. Pachla, J. Smalc-Koziorowska, S. Przybysz, and M. Przybysz

Fig. 10. Grain size distribution for (a) AA5083 alloy after the cumulative cold HE hydrostatic extrusion with cumulative true strains $\varepsilon_{cum} = 2.95$ and $\varepsilon_{cum} = 3.9$, and (b) AA5754 alloy after the two-step ECAP process by C route and single- and two-step cold hydrostatic extrusion with cumulative true strains $\varepsilon_{cum} = 3.3$ and $\varepsilon_{cum} = 4.3$

hydrostatic extrusion with strain $\varepsilon_{cum} = 2.95$, strong microstructure refinement is observed, to average grain size $d_{eq} \sim 150$ nm (Fig. 9b). There are also locally visible high defect density areas with a poorly developed UFG ultra-fine grain structure, (Fig. 9c). The strongest effect of microstructure refinement to $d_{eq} \sim 140$ nm is observed after maximum strain $\varepsilon_{cum} \sim 3.9$, with no underdeveloped grain areas and the structure is uniform throughout the volume (Fig. 9d). Reflections in the inserted diffraction image are arranged in concentric rings, which indicates a uniform distribution of the observed grains' orientation. The effect of refinement and homogenization of the microstructure after the last HE step is illustrated by the grain size distribution shown in Fig. 10a, where the larger 250–300 nm fraction disappears and the smaller 50–150 nm fraction increases. The initial AA5754 alloy was characterized by a coarse grained structure with an average grain size $d_{eq} \sim 70$ µm (Fig. 11a). The material
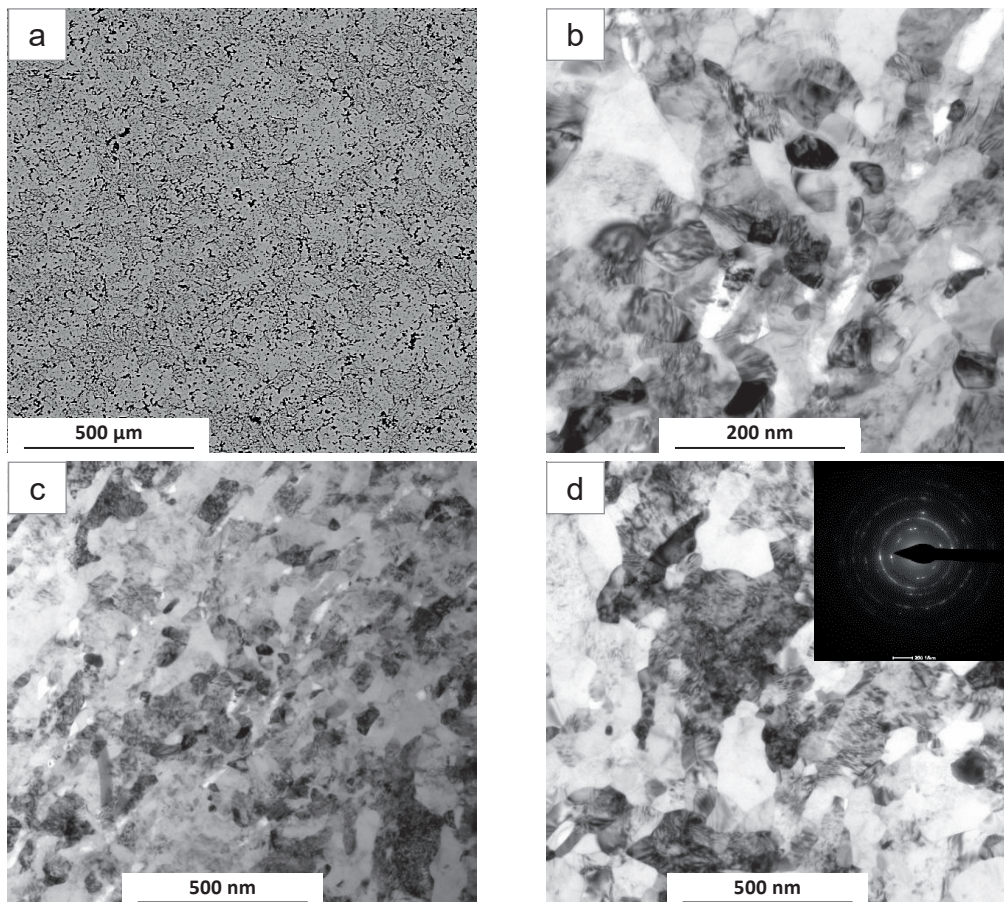

Fig. 11. AA5754 alloy microstructure on the cross-section of the rod (a) in the initial state, (b) and (c) after the ECAP by C route and one-step cold HE hydrostatic extrusion with cumulative true strain $\varepsilon_{cum} = 3.3$, and (d) after the ECAP process as (b) and (c) and two-step HE with strain $\varepsilon_{cum} = 4.3$

www.czasopisma.pan.pl   PAN   www.journals.pan.pl
POLSKA AKADEMIA NAUK

The effect of high-pressure plastic forming on the structure and strength of AA5083 and AA5754 alloys intended for fasteners

after the two ECAP C route passes and the one-step cold HE with strain $\varepsilon_{cum} = 3.3$ is characterized by a homogeneous structure in the whole volume with average grain size $d_{eq} = 130$ nm (Fig. 11b and c). After adding the second HE step and increasing the strain to $\varepsilon_{cum} = 4.3$, the grain size slightly decreases to $d_{eq} = 125$ nm, and the developed fine-grained structure, like that of AA5083 alloy, is clearly visible (Fig. 11d). The slight shift in grain size towards smaller fractions at the strain increase for AA5754 alloy is shown in Fig. 10b.

According to the literature data, four ECAP *Bc* route passes only produce grains with the average size of ~300–400 nm with indistinctly formed boundaries [16]. Only six passes ($\varepsilon_{cum} \sim 6$) produce a structure with clearly developed grains with high-angle boundaries. In this study, despite the smaller cumulative strain $\varepsilon_{cum} = 4.3$ a much stronger refinement effect up to 125 nm and homogenization of the microstructure is observed (Fig. 11d). This results from the combination of the initial ECAP with the later HE, which leads to a change in the deformation route and more effective generation of defects in the plastic deformation process, and consequently to a stronger microstructure refinement.

The effect of combining the ECAP and HE methods was described in earlier works, e.g. for AA5483 alloy, where grain size $d_{eq} = 70$ nm was obtained with cumulative strain $\varepsilon_{cum} = 5.9$ [4], and for CuCrZr copper alloy, where $d_{eq} = 200$ nm with cumulative strain $\varepsilon_{cum} = 11.5$ was obtained [22].

3.5 Fastener thread profile. The AA5083 alloy threads were burnished and cut in the material's initial state and after the cold HE hydrostatic extrusion with strain $\varepsilon_{cum} = 1.64$. M30 threads standardized as per PN-ISO 965-2: 2001 were tested. Figure 12 shows the results of measurements of the pitch diameter of the burnished threads in relation to the minimum and maximum values required by the standard. The material after HE within
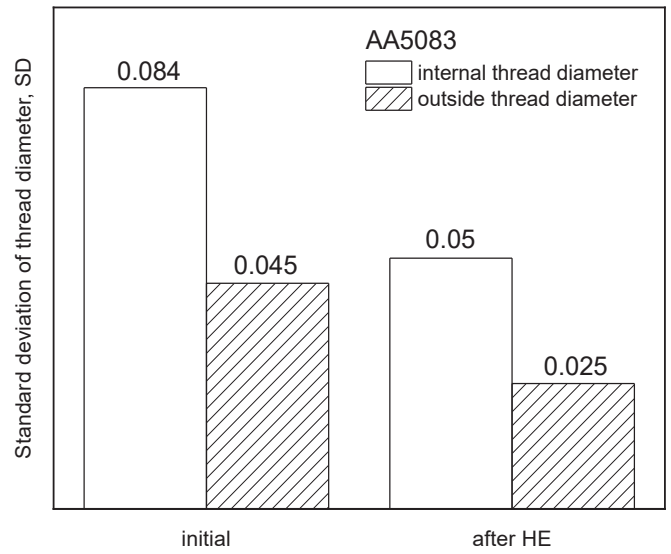

Fig. 13. Standard deviation of the burnished thread's outer and inner diameters for AA5083 alloy in the initial state and after the cold HE hydrostatic extrusion

the whole measuring range stays within standardised values. Due to its lower mechanical properties and the resultant high susceptibility to plastic deformation, the pitch diameter of the initial material thread at the beginning of the thread lies below the minimum standardised values and in the entire measuring range increases to the end of the thread. The results of the thread's outer and inner diameter deviations for AA5083 alloy indicate almost double threading accuracy after the HE compared to the initial material (Fig. 13).

Figure 14 shows the measurements of the cut threads' pitch diameters for AA5083 alloy in the initial state and after the
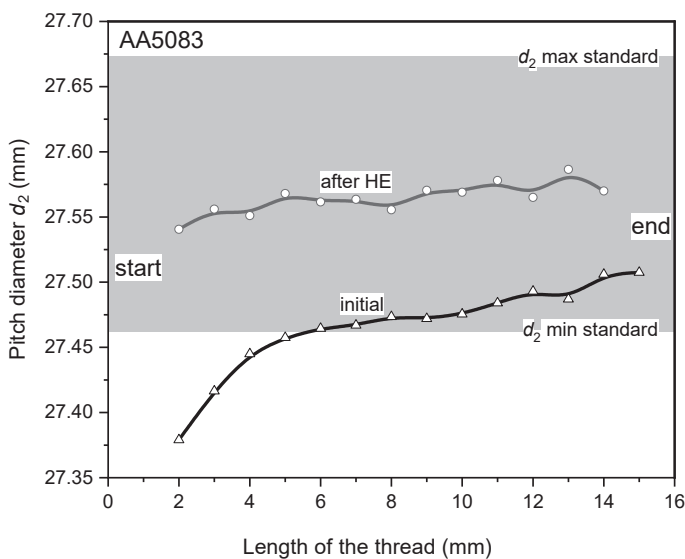

Fig. 12. Changes in pitch diameter in relation to normalized values over the length of burnished threads of commercial alloy AA5083 and after the cold HE hydrostatic extrusion
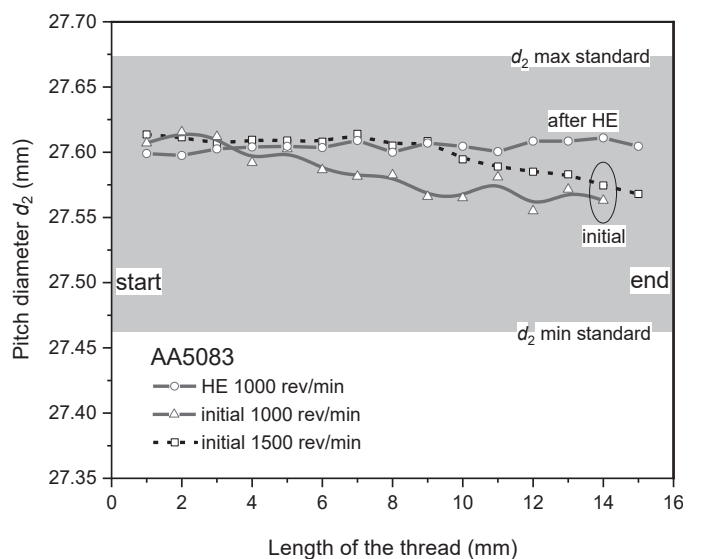

Fig. 14. Dimensions of the pitch diameter over the length of the thread cut in the initial AA5083 material at 1000 and 1500 rev/min and in the alloy after the cold HE hydrostatic extrusion at 1000 rev/min

M. Kulczyk, J. Skiba, W. Pachla, J. Smalc-Koziorowska, S. Przybysz, and M. Przybysz

HE hydrostatic extrusion for the initial material, cutting speeds were 1000 and 1500 rev/min, and 1000 rev/min for the material after HE. The results for the initial material are much more heterogeneous, and the pitch diameter decreases over the entire thread length. Numerous defects were observed on the surface of the threads cut in the initial AA5083 material at rotational speed 1000 rev/min (Fig. 15a). Good surface quality is achieved only at 1500 rev/min (Fig. 15b), while after HE the correct thread profile is obtained at much lower speed 1000 rev/min (Fig. 15c), which translates directly into less wear of the threading tools.

4. Conclusions

The paper examined the effect of severe plastic deformations by the hydrostatic extrusion method on the mechanical and structural properties of AA5083 and AA5754 aluminium alloys with magnesium. In both materials, much higher mechanical properties were obtained compared to the initial materials. For AA5083 alloy after the HE cumulative process with total true strain $\varepsilon_{cum} = 3.9$ they were YS = 500 MPa and UTS = 510 MPa, respectively, and for AA5754 alloy after the combination of ECAP and HE with total true strain $\varepsilon_{cum} = 4.3$ – YS = 440 MPa and UTS = 450 MPa, respectively. This means an increase compared to the initial material, by 175% and 45%, respectively for AA5083 alloy, and by 175% and

60%, respectively, for AA5754 alloy. This effect is due to the microstructure homogenisation and strong refinement to the grain sizes $d_{eq} = 140$ nm and $d_{eq} = 125$ nm, respectively, and the adiabatic heating effect minimisation by the cumulative HE hydrostatic extrusion and ECAP methods. After the cumulative deformation and combined HE and ECAP treatment the YS yield strengths are closer to UTS strength, which means that a fastener made of such material can be safely loaded to the maximum allowed by its strength. The resultant mechanical properties allow to replace the strongest aluminium alloys with zinc series AA7075 with Al-Mg alloys in critical structures, especially due to their much better corrosion resistance. The tests of thread profiles of fasteners made of the AA5083 alloy after HE shows higher threading accuracy and the possibility of using lower cutting speeds, which reduces the tool wear.

References

[1] S. Mousavi, M. Khaleghifar, M. Meratian, B. Sadeghi, and P. Cavaliere, "Effect of the equal channel angular pressing route on the microstructural and mechanical behavior of Al-5086 alloy", *Materialia,* 4, 310–322 (2018).
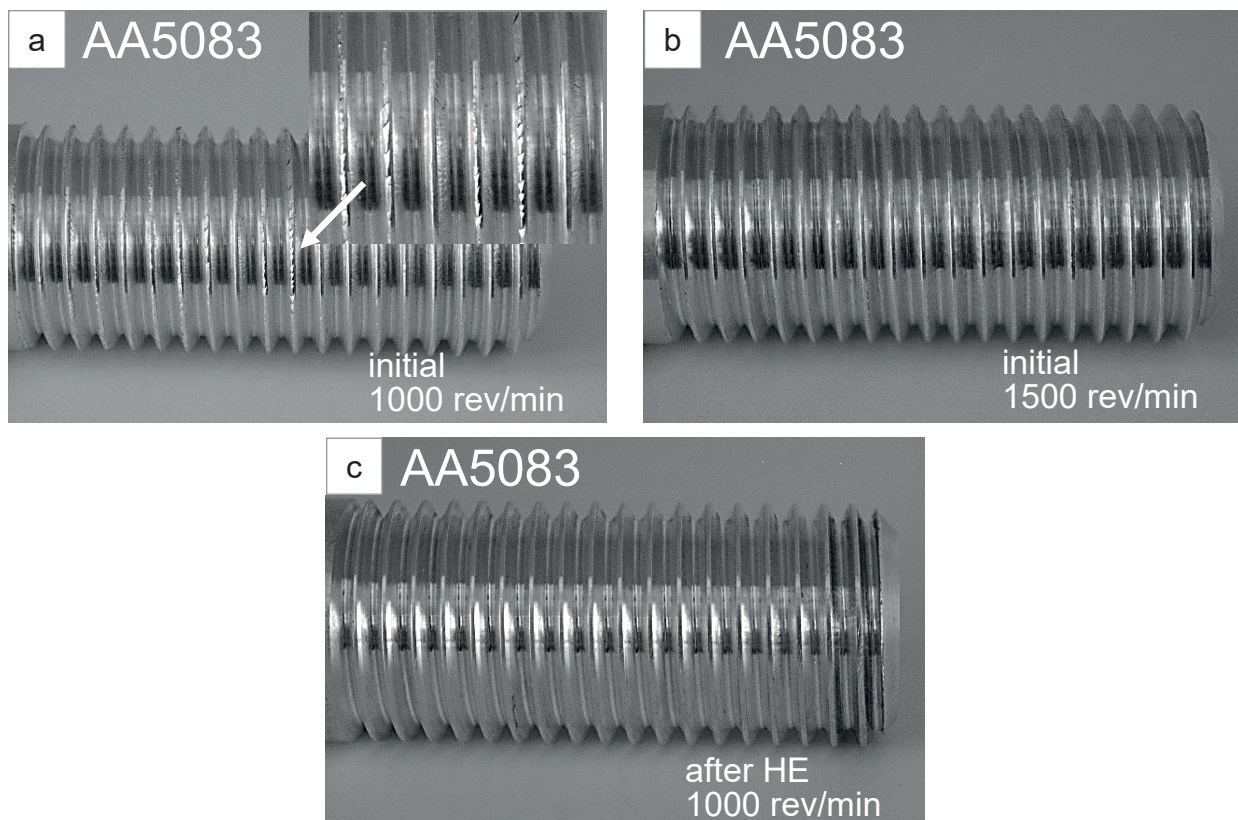
Fig. 15. Threads cut in AA5083 alloy in the initial state at rotational speeds (a) 1000 rev/min and (b) 1500 rev/min, and (c) after the HE cold hydrostatic extrusion at 1000 rev/min

[2] L. Tan and T.R. Allen, "Effect of thermomechanical treatment on the corrosion of AA5083", *Corros. Sci*. 52, 548–554 (2010).

[3] P. Bazarnik, M. Lewandowska, M. Andrzejczuk, and K.J. Kurzydlowski, "The strength and thermal stability of Al–5Mg alloys nano-engineered using methods of metal forming", *Mater. Sci. Eng*. A 556, 134–139 (2012).

[4] M. Kulczyk, J. Skiba, and W. Pachla, "Microstructure and mechanical properties of AA5483 treated by a combination of ECAP and hydrostatic extrusion", *Arch. Metall. Mater.* 59, 163–166 (2014).

[5] http://www.mettex.co.uk/product-groups/fasteners/

[6] Y. Liu, M. Liu, X. Chen, Y. Cao, H. J. Roven, M. Murashkin, R. Z.Valiev, and H. Zhou, "Effect of Mg on microstructure and mechanical properties of Al-Mg alloys produced by high pressure torsion", *Scr. Mater.* 159, 137–141 (2019).

[7] M. Kulczyk, J. Skiba, S. Przybysz, W. Pachla, P. Bazarnik, and M. Lewandowska, "High strength silicon bronze (C65500) obtained by hydrostatic extrusion", *Arch. Metall. Mater*. 57, 859–862 (2012).

[8] W. Pachla, M. Kulczyk, A. Mazur, and M. Sus-Ryszkowska, "UFG and nanocrystalline microstructures produced by hydrostatic extrusion of multifilament wires", *Int. J. Mater. Res*. 100, 984–990 (2009).

[9] M. Kulczyk, W. Pachla, J. Godek, J. Smalc-Koziorowska, J. Skiba, S. Przybysz, M. Wróblewska, and M. Przybysz, "Improved compromise between the electrical conductivity and hardness of the thermo-mechanically treated CuCrZr alloy", *Mater. Sci. Eng. A* 724, 45–52 (2018).

[10] W. Pachla, A. Mazur, J. Skiba, M. Kulczyk, and S. Przybysz, "Wrought magnesium alloys ZM21, ZW3 and WE43 processed by hydrostatic extrusion with back pressure", *Arch. Metall. Mater*. 57, 485–493 (2012).

[11] W. Pachla, M. Kulczyk, S. Przybysz, J. Skiba, K. Wojciechowski, M. Przybysz, K. Topolski, A. Sobolewski, and M. Charkiewicz, "Effect of severe plastic deformation realized by hydrostatic extrusion and rotary swaging on the properties of CP Ti grade 2", *J. Mater. Process. Technol.* 221, 255–268 (2015).

[12] M. Kulczyk, W. Pachla, A. Mazur, M. Sus-Ryszkowska, N. Krasilnikov, and K.J. Kurzydłowski, "Producing bulk nanocrystalline materials by combined hydrostatic extrusion and equal channel angular pressing", *Mater. Sci. Poland* 25(4), 991–999 (2007).

[13] W. Pachla, J. Skiba, M. Kulczyk, S. Przybysz, M. Przybysz, M. Wróblewska, R. Diduszko, R. Stępniak, J. Bajorek, M. Radomski, and W. Fąfara, "Nanostructurization of 316L type austenitic stainless steels by hydrostatic extrusion", *Mater. Sci. Eng. A* 615, 116–127 (2014).

[14] S. Przybysz, M. Kulczyk, W. Pachla, J. Skiba, M. Wróblewska, J. Mizera, and D. Moszczyńska, "Anisotropy of mechanical and structural properties in AA 6060 aluminum alloy following hydrostatic extrusion process", *Bull. Pol. Ac.: Tech*. 67(4), 709–717 (2019).

[15] N. Izairi, F. Ajredini, A. Veveçka-Priftaj, and M. Ristova, "Enhancement of mechanical properties of the AA5754 aluminum alloy with a severe plastic deformation", *Materials and Technology* 48(3), 385–388 (2014).

[16] A. Veveçka, P. Cavaliere, M. Cabbibo, E. Evangelista, and T.G. Langdon, "Strengthening of a commercial Al-5754 alloy using equal-channel angular pressing", *J. Mater. Sci. Lett*. 20, 1601–1603 (2001).

[17] S.-Y. Changa, B.-D. Ahnb, S.-K. Hongc, S. Kamadod, and Y. Kojimad, "Dong Hyuk Shin Tensile deformation characteristics of a nano-structured 5083 Al alloy", *J. Alloy. Compd*. 386, 197–201 (2005).

[18] J.S. Choi, S. Nawaz, S.K. Hwang, H.C. Lee, and Y.T. Im, "Forgeability of ultra-fine grained aluminum alloy for bolt forming", *Int. J. Mech. Sci.* 52, 1269–1276 (2010).

[19] J.H. Kim, S.K. Hwang, Y.T. Im, I.H. Son, and C.M. Bae, "High-strength bolt-forming of fine-grained aluminum alloy 6061 with a continuous hybrid proces" , *Mater. Sci. Eng. A* 552, 316–322 (2012).

[20] J.S. Choi, Y.G. Jin, H.C. Lee, and Y.T. Im, "High strength bolt manufacturing of ultra-fine grained aluminium alloy 6061", Materials Transactions, 52(2), 173–178 (2011).

[21] T. Wejrzanowski, W.L. Spychalski, K. Różniatowski, and K.J. Kurzydłowski, "Image based analysis of complex microstructures of engineering materials", *Int. J. Appl. Math. Comput. Sci*. 18(1), 33–39 (2008).

[22] M. Kulczyk, B. Zysk, M. Lewandowska, and K. J. Kurzydlowski, "Grain refinement in CuCrZr by SPD processing", *Phys. Status Solidi A*, 207(5), 1136–1138 (2010).